

“Rosenbluth” separation of the  $J/\psi$  near-threshold photoproduction - an access to the  
gluon Gravitational Form Factors at high  $t$

Lubomir Pentchev\* and Eugene Chudakov†

### Abstract

We perform analysis of the near-threshold  $J/\psi$  photoproduction data off the proton based on two theoretical approaches, GPD [1] and holographic [2], that represent the differential cross sections as powers of the skewness parameter with coefficients that depend only on the momentum transfer  $t$ . This allows to separate kinematically the corresponding coefficient functions, in much the same way as this is done for the electric and magnetic form factors using the Rosenbluth separation. We examine the independence of the extracted functions with the photon beam energy. These functions, under additional assumptions, are related to the proton’s gluon Gravitational Form Factors (gGFFs). We compare the extracted functions with lattice calculations of the gGFFs in the region of  $0.5 < |t| < 2 \text{ GeV}^2$ , where they overlap. Such analysis demonstrates the possibility of extracting some combinations of the gGFFs from the data at high  $t$ , complementary to the lattice calculations available in the low  $t$  region. However, higher statistics are needed to more accurately check the predicted scaling behavior of the data and compare with the lattice results, thus testing and comparing the theoretical assumptions used in the GPD and holographic models.

---

\* Thomas Jefferson National Accelerator Facility, Newport News, Virginia 23606, USA; pentchev@jlab.org

† Thomas Jefferson National Accelerator Facility, Newport News, Virginia 23606, USA; gen@jlab.org

## I. INTRODUCTION

Charmonium photoproduction near threshold provides a unique way to probe the gluonic structure of the nucleon. Due to the high mass of the charm quark and proximity to the threshold, the reaction is expected to be dominated by two-gluon exchange [3, 4]. In the GPD approach factorization is assumed based on the high charmonium mass defining the hard scale in the reaction [5, 6]. As the two gluons can mimic graviton-like exchange, the gluonic GPD in turn can be related to the gluon Gravitational Form Factors (gGFFs) [5, 7]. To be able to access the gluonic content of the nucleon, the above chain of assumptions requires experimental testing.

In the recent years, thanks to the 12 GeV Jefferson Lab electron accelerator, several experiments measured the  $J/\psi$  photoproduction near threshold with much higher precision than the previous experiments from the 1970s. The GlueX experiment in Hall D performed measurements with a nearly full acceptance spectrometer in a wide range of photon beam energies starting from the threshold of 8.2 GeV to the maximum available energy of about 11.8 GeV [8, 9]. In addition to the total cross-section, the differential cross sections were extracted in three slices of the photon beam energy, providing full coverage of the near-threshold kinematic region. The  $J/\psi$ -007 experiment in Hall C accumulated similar statistics in a narrower kinematic region with several settings of their two low-acceptance spectrometers that however allowed very high luminosity [10]. The differential cross sections were measured in 10 narrow energy bins with very high statistics in the forward region.

In Ref. [10] the gGFFs have been extracted by fitting the  $J/\psi$ -007 data with the theoretical predictions from the holographic [2] and GPD [5] approaches. In the GPD analysis of Ref. [6], the data from both GlueX and  $J/\psi$ -007 experiments were used to extract the gGFFs. The GPD approach is based on expansion in the skewness parameter  $\xi$  for values approaching unity (see also [7]). Therefore its validity is justified for high  $|t|$  values due to kinematic correlation between  $t$  and  $\xi$ . A common feature of the above two analyses in Refs. [6, 10] is the modeling of the gGFFs with dipole/tripole functions. The dipole form was proposed in Ref. [11] in analogy with the electro-magnetic form factors, whereas the tripole one is a good approximation of the holographic results [2]. Such functional forms are consistent with the

lattice calculations in Refs. [12, 13] and used there as a parametrization of the results. While the GPD approach works at high  $|t|$ , the lattice calculations of the gGFFs have been done so far in the  $0 < |t| < 2 \text{ GeV}^2$  region. Therefore, the use of dipole/tripole parametrization especially at high  $|t|$  requires experimental validation. Most importantly, the extraction of the gGFFs in both analysis of Refs. [6, 10] is guided by additional external constraints on some of the gGFF parameters, based on, or consistent with the lattice calculations. As a result, first, the extracted gGFFs are sensitive to the normalization of the theoretical models and second, when compared to the lattice calculations, such results are not completely independent.

The analysis in this work is based on one of the important results of Ref. [1], that the differential cross section of the charmonium photoproduction for high  $\xi$  values can be presented in this general form:

$$d\sigma/dt \sim \xi^{-4} [G_0(t) + \xi^2 G_2(t) + \xi^4 G_4(t)], \quad (1)$$

where the coefficients  $G_0$ ,  $G_2$ , and  $G_4$  are functions only of  $t$ , which in the leading-moment approximation are related to the gGFFs. The holographic theory in Ref. [2] gives a similar expression:

$$d\sigma/dt \sim [A_g(t) + \eta^2 4C_g(t)]^2, \quad (2)$$

making direct connection to the gravitational form factors  $A_g(t)$  and  $C_g(t)$ , where  $\eta$  has a similar meaning as the skewness parameter  $\xi$ . It is important to stress that the GPD and holographic theories have very different domains of validity. The holographic theory is valid for soft processes because it works in the limit of high coupling constant. In contrast the GPD theory requires high  $|t|$  and works for hard processes. We aim to extract the  $t$ -functions in Eqs.(1,2) (we will call them form factor functions) from the experimental data without any additional assumptions. In contrast to the studies in Refs. [6, 10], **first, the procedure described in this work does not use any external constraints and second, the results will not be model functions fitted to the data, but actual data points measuring the absolute value and  $t$ -dependence of the above form factors.**

We point out the analogy with the Rosenbluth separation of the electric,  $G_E$ , and magnetic,  $G_M$ , form factors. Based on the Rosenbluth formula [14] for the electron-proton elastic cross section,  $d\sigma/d\Omega$ , the method relies on the linear dependence of the reduced cross section,  $\sigma_R$ , on the kinematic variable  $\epsilon$ :

$$\sigma_R = \frac{d\sigma}{d\Omega} / \left( \frac{d\sigma}{d\Omega} \right)_M \frac{\epsilon(1 + \tau)}{\tau} = \frac{\epsilon}{\tau} G_E^2(t) + G_M^2(t), \quad (3)$$

where  $\left( \frac{d\sigma}{d\Omega} \right)_M$  is the Mott cross section,  $\tau = -t/4m^2$ , where  $m$  is the proton mass. By measuring  $\sigma_R$  at the same momentum transfer  $t$  as function of  $\epsilon/\tau$ , one can estimate the slope and the intercept, being respectively the electric and magnetic form factors squared at this value of  $t$ .

The analogy of Eqs.(1,2) with Eq.(3) is clear: instead of  $\epsilon$ , we can use the variations with  $\xi$  or  $\eta$  at a fixed  $t$  to extract the form factor functions in Eq.(1,2). In this paper we will apply a similar ‘‘Rosenbluth’’ technique, however with some noticeable differences. Due to the limited experimental data so far, it is practically impossible to analyze separately data sets in narrow ranges of  $t$  versus some function of  $\xi$  or  $\eta$ . The GPD analysis has additional complications due to high  $\xi$  requirement and the kinematic constraints that impose correlations between the ranges of  $t$  and  $\xi$ .

In our analysis we will use the results from the two Jefferson Lab experiments, GlueX and  $J/\psi$ -007, and in case of the GPD, selecting data points with  $\xi > 0.4$ . Such limit may not be high enough for the assumptions in Ref. [1] to be valid, and the selection is driven by the limited amount of data at high  $\xi$ . In addition we will select measurements with photon energies above 9.3 GeV, to stay away from the open-charm thresholds of  $\Lambda_c \bar{D}$  and  $\Lambda_c \bar{D}^*$ . As discussed recently in Refs.[9, 15, 16], there is possible evidence for contributions from reactions with open-charm exchange.

In section II we will formulate the ‘‘Rosenbluth’’ technique. It will be used in section III to extract the form factor functions and check their energy independence. In section IV we will work within the leading-term approximation to demonstrate the possibility of extracting some combinations of the gGFFs and compare them to the lattice results. Some additional remarks and summary will be given in section V.

## II. THE ‘‘ROSENBLUTH’’ TECHNIQUE

In the GPD calculations of Ref. [1] the differential cross section of the  $J/\psi$  photoproduction near threshold is presented as a function of the skewness parameter  $\xi$  and the momentum transfer  $t$ :

$$\frac{d\sigma}{dt}(\xi, t) = F(E) \cdot \xi^{-4} [G_0(t) + \xi^2 G_2(t) + \xi^4 G_4(t)], \quad (4)$$

where the factor  $F$  includes a kinematic factor and the  $J/\psi$  non-relativistic wave function at origin, and depends only on the photon beam energy,  $E$ , while the  $G$  functions depend only on  $t$ . The skewness is defined as:

$$\xi = \frac{M^2 - t}{2(s - m^2) - M^2 + t}, \quad (5)$$

where  $M$  and  $m$  correspond to the  $J/\psi$  and the proton masses and  $s$  is the center of mass energy squared. The  $G$  functions are given by:

$$G_0(t) = (\mathcal{A}_g(t))^2 - \frac{t}{4m^2} (\mathcal{B}_g(t))^2 \quad (6)$$

$$G_2(t) = 2\mathcal{A}_g(t)\mathcal{C}_g(t) + 2\frac{t}{4m^2}\mathcal{B}_g(t)\mathcal{C}_g(t) - (\mathcal{A}_g(t) + \mathcal{B}_g(t))^2 \quad (7)$$

$$G_4(t) = \left(1 - \frac{t}{4m^2}\right) (\mathcal{C}_g(t))^2. \quad (8)$$

In the leading-moment approximation the functions  $\mathcal{A}_g$ ,  $\mathcal{B}_g$ , and  $\mathcal{C}_g$  are related to the gluonic Gravitational Form Factors (gGFF)  $A_g$ ,  $B_g$ , and  $C_g$  as:

$$\mathcal{A}_g(t) = 2A_1^{conf} A_g(t) \quad (9)$$

$$\mathcal{B}_g(t) = 2A_1^{conf} B_g(t) \quad (10)$$

$$\mathcal{C}_g(t) = 8A_1^{conf} C_g(t), \quad (11)$$

using the conformal expansion of the above functions, where  $A_1^{conf} = 5/4$  [1].

The holographic approach of Ref. [2] gives direct relation between the cross section and the

gravitational form factors  $A_g$  and  $C_g$ :

$$\frac{d\sigma}{dt}(\eta, t) = N(E) [A_g(t) + \eta^2 4C_g(t)]^2, \quad (12)$$

where

$$\eta = \frac{M^2}{2(s - m^2) - M^2 + t}, \quad (13)$$

In this approach the  $B_g$  form factor is zero. The  $N(E)$  function is normalized using GlueX total cross section, which is in contrast to the GPD calculations that are absolute. The holographic theory is valid in the double limit of strong gauge coupling and large number of colors,  $N_c$ . To indicate the approximate nature of the results we will rewrite the above formula in analogy with Eq.(4) as:

$$\frac{d\sigma}{dt}(\eta, t) = N(E) [H_0(t) + \eta^2 H_2(t) + \eta^4 H_4(t)], \quad (14)$$

where in the limit of the validity of the theory we have:

$$H_0(t) = A_g^2(t) \quad (15)$$

$$H_2(t) = 8A_g(t)C_g(t) \quad (16)$$

$$H_4(t) = 16C_g^2(t), \quad (17)$$

In the GPD case we will renormalize the  $G$  functions in Eq.(4) as:

$$\frac{d\sigma}{dt}(\xi, t) = F(E) \cdot 4(A_1^{conf})^2 \xi^{-4} [G_0(t) + \xi^2 G_2(t) + \xi^4 G_4(t)], \quad (18)$$

so that in the leading-moment approximation, Eqs.(6-11), when neglecting  $B_g$ , the  $G_0$  and  $H_0$  function have the same normalization, in which case we have similar relations to the

gGFFs:

$$G_0(t) = A_g^2(t) \quad (19)$$

$$G_0(t) + G_2(t) = 8A_g(t)C_g(t) \quad (20)$$

$$G_4(t) = 16C_g^2(t) \left(1 - \frac{t}{4m^2}\right). \quad (21)$$

Thus, in the further formulas we will attach the factor  $4(A_1^{conf})^2$  to the  $F(E)$  function.

We will derive the equations for the ‘‘Rosenbluth’’ separation in the GPD case only. The formulas for the holographic approach can be derived in much the same way and the results will be shown later. From Eqs.(18) we construct the reduced cross section:

$$\sigma_{R0}(E, t) = \frac{d\sigma}{dt}(E, t) \frac{\xi^2(E, t)}{F(E)} = \xi^{-2}(E, t)G_0(t) + G_2(t) + \xi^2(E, t)G_4(t), \quad (22)$$

where we have indicated the energy and  $t$  dependence of the corresponding variables<sup>1</sup>. We have verified, initially based on the lattice results from Refs. [12, 13] discussed later, that the last term in Eq.(18), and respectively Eq.(22), is much smaller in absolute value than each of the other two terms. Partially this is because of the  $\xi^4/\xi^2$  suppression factor (as  $\xi < 1$ ) with respect to the first/second term. This assumption will be checked later based on the results of this analysis. Note that this does not necessarily mean that the last terms in Eqs.(18) and (22) can be neglected. It will be shown that the other two terms have different signs and it is possible they largely cancel each other.

The second term in Eq.(22) depends only on  $t$  and we can eliminate it by taking the difference of the cross sections at two different photon energies,  $E_i$  and  $E_j$ :

$$\begin{aligned} \sigma_{R0}(E_i, t) - \sigma_{R0}(E_j, t) &= [\xi^{-2}(E_i, t) - \xi^{-2}(E_j, t)] G_0(t) \\ &+ [\xi^2(E_i, t) - \xi^2(E_j, t)] G_4(t). \end{aligned} \quad (23)$$

Now the last term can be neglected with respect to the first one, and we have the  $G_0$  function

---

<sup>1</sup> Note that all reduced cross sections defined in this work are dimensionless quantities

extracted from experimental data:

$$G_0^{exp.}(t) = [\sigma_{R0}(E_i, t) - \sigma_{R0}(E_j, t)] / [\xi^{-2}(E_i, t) - \xi^{-2}(E_j, t)] \quad (24)$$

We will choose a data set at a given energy  $E_i$  as a reference. Thus, the above equation will give us the slope of the reduced cross section as function of  $\xi^{-2}$  for each additional data point with transfer momentum  $t$  and energy  $E_j$  with respect to the reference energy, which is the  $G_0(t)$  function and should not depend on the energy  $E_j$ . Thus, checking the energy independence of the extracted form factor function will serve as a test of the validity of the  $\xi$ -scaling as given by Eq.(1). With this method the uncertainties of the reference data set can be considered to be systematic errors common for all data points.

The  $G_2(t)$  function can be extracted in much the same way. Here we give as an example the formulas for the sum  $G_0(t) + G_2(t)$  that enters in Eq. (20):

$$(G_0(t) + G_2(t))^{exp.} = [\sigma_{R02}(E_i, t) - \sigma_{R02}(E_j, t)] / \left[ \frac{\xi^2(E_i, t)}{1 - \xi^2(E_i, t)} - \frac{\xi^2(E_j, t)}{1 - \xi^2(E_j, t)} \right], \quad (25)$$

where we have defined another reduced cross section as:

$$\sigma_{R02}(E, t) = \frac{d\sigma}{dt}(E, t) \frac{\xi^4(E, t)}{F(E)(1 - \xi^2(E, t))}. \quad (26)$$

### III. ENERGY INDEPENDENCE OF THE FORM FACTOR FUNCTIONS

#### A. The GPD approach

The practical implementation of the above technique is limited by the quality and range of the available data. The data sets from the two Jefferson Lab experiments are illustrated in Fig.1. As discussed above for the main part of the GPD analysis we will use the data with  $\xi > 0.4$  and  $E > 9.3$  GeV. This region on the  $E$ -vs- $t$  plane in Fig.1 is shown with color. We will choose the highest energy data set from the GlueX experiment, at an average energy  $E_i = 10.82$  GeV, as a reference and subtract the other data at different energies  $E_j$ . Such a



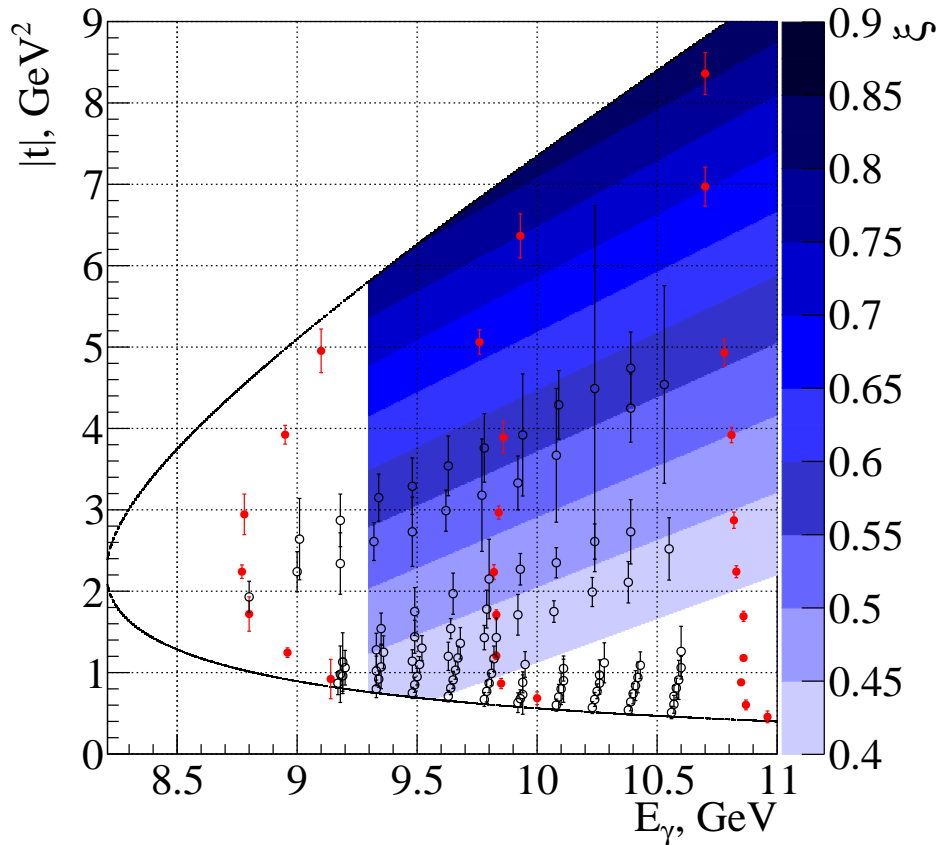


FIG. 1: Data points of the GlueX [9] (red solid) and  $J/\psi$ -007 [10] (black open) experiments on the  $E$ -vs- $t$  plane. The vertical error bars represent the relative errors of the differential cross sections measured at these points in arbitrary units (not related to the  $y$  axis). The  $\xi$  values on this plot are given on the  $z$ -axis (color coded). Some of the  $J/\psi$ -007 points are slightly shifted up in energy for visibility. The colored (shaded in print) area corresponds to the  $\xi > 0.4$  and  $E > 9.3$  GeV region that is used in the GPD analysis. In the holographic case all the data points for  $E > 9.3$  GeV are used.

choice gives maximum leverage in  $\xi$  when calculating the slopes from Eqs.(24) and (25), at the same time the highest energy data set is more precise and has the widest range in  $t$ .

In principle, we can fit only the reference cross section with some function, so that we can use it in Eqs.(24) and (25) to subtract the reduced cross sections at the  $t$  values of the data points at the other energies. Still, as seen in Fig.1, due to the  $\xi > 0.4$  constraint, the  $1 - 2$  GeV<sup>2</sup> region in  $|t|$  is not covered by the reference cross section, therefore it requires extrapolation to lower  $|t|$ . For that we will fit all the cross sections simultaneously using Eq. (18). Thus, the extrapolation of the reference energy will be guided by the data at the

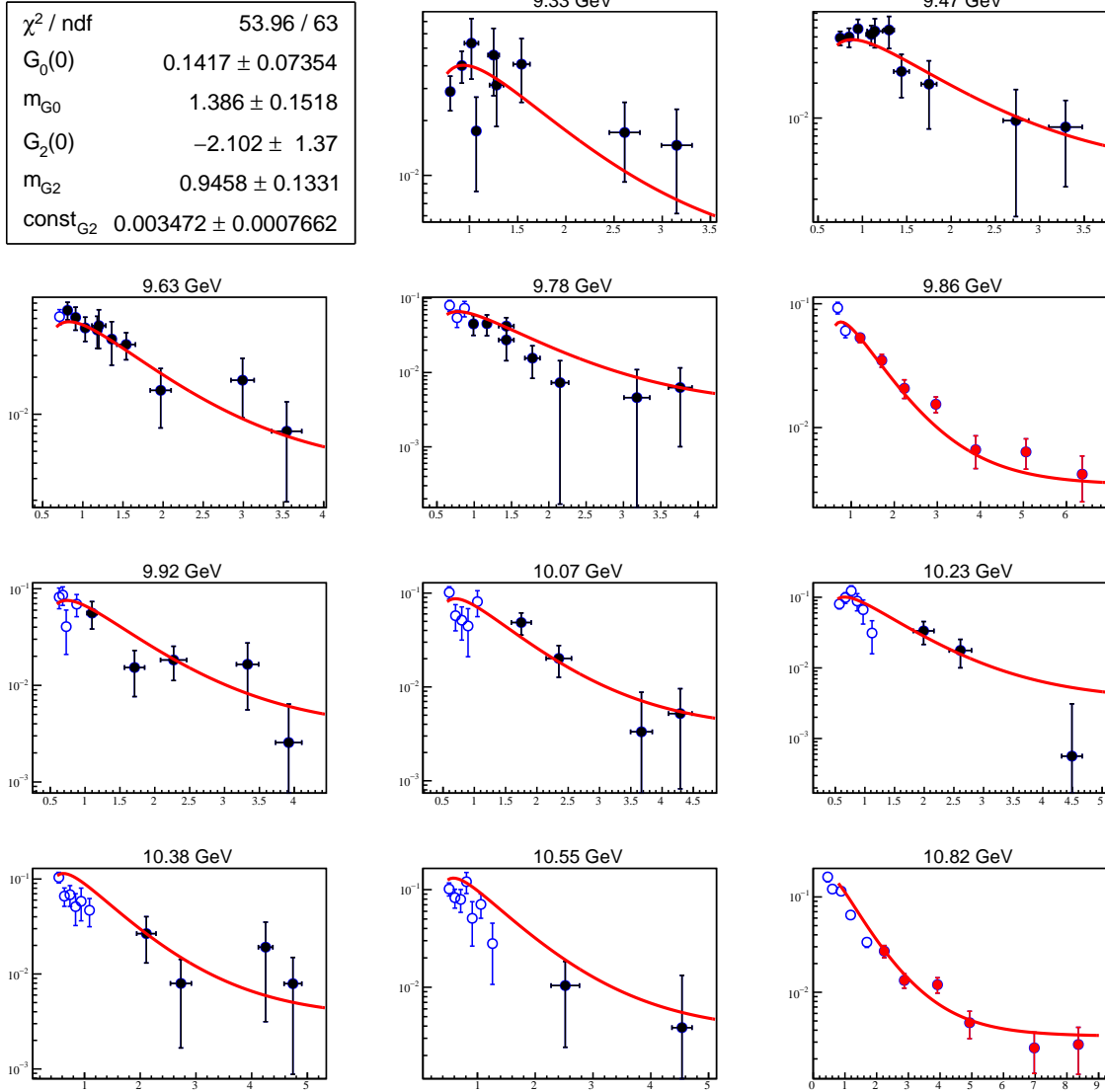


FIG. 2: Global five-parameter fit of the reduced cross sections,  $\xi^2/F \cdot d\sigma/dt$ , as function of  $|t|$  (in  $\text{GeV}^2$ ), using the GPD Eq.(18) and the parametrizations given by Eqs. (27,28), from GlueX (red) and  $J/\psi$ -007 (black) experiments for different photon energies as indicated.

The data points with  $\xi < 0.4$  are plotted (blue) but not used in the fit. For the further analysis only the fitted function at 10.82 GeV is used.

other energies, at the same time reducing the error of the function fitted to the reference energy.

We demonstrate this procedure when fitting the reduced cross section,  $\sigma_{R0}$ , as function of  $t$  for all energies using Eq. (18). Good fit results are obtained if we neglect  $G_4$  and parametrize

$G_0$  and  $G_2$  with squared dipole functions:

$$G_0(t) = \frac{G_0(0)}{(1 + t/m_{G_0})^4} \quad (27)$$

$$G_2(t) = \frac{G_2(0)}{(1 + t/m_{G_2})^4} + \text{const}_{G_2}, \quad (28)$$

where the constant term added for  $G_2$  improves the fit quality for  $|t| > 5 \text{ GeV}^2$ . The fit results are shown in Fig.2. The data points for  $\xi < 0.4$ , also plotted in the figure but not used in the fit, deviate from the fitted functions. In the further analysis for the extraction of  $G_0^{exp.}(t)$ , in Eq.(24) we will use only the fitted function for the reference energy  $E_i = 10.82 \text{ GeV}$  (Fig.2 bottom right).

To illustrate clearly how the ‘‘Rosenbluth’’ technique works, in Fig. 3 we show the different stages of the extraction of the  $G_0(t)$  function from the GlueX data. Here, just for this demonstration, we have included the differential cross section at the lowest beam energy. Starting from the original cross sections, going to the  $\xi$ -scaled cross sections, and finally calculating the slopes from Eq.(24), it is remarkable to see how the results at the different energies converge into a function,  $G_0^{exp.}(t)$ , that is largely energy independent.

The results for  $G_0$  and the sum  $G_0 + G_2$  using all the data are shown in Figs. 4a and 4b. For better comparison of the two results, we have divided the sum by 8 - see Eqs.(19,20). We see that the extracted functions do not depend on energy within the experimental errors. Numerically, this is confirmed by the good quality of the fits of all the data using squared dipole functions. The uncertainties of the fitted function at the reference energy (as in Fig. 2 bottom right panel) are scaled by the factors in Eqs.(24,25) and shown in Figs.4a and 4b as global systematic errors.

## B. Holographic approach

The formulas for extracting the  $H_0$  and  $H_2$  form factor functions are the same as for  $G_0$  and  $G_2$  when replacing  $\xi$  by  $\eta$ , except for the definition of the reduced cross sections. The  $H_0$

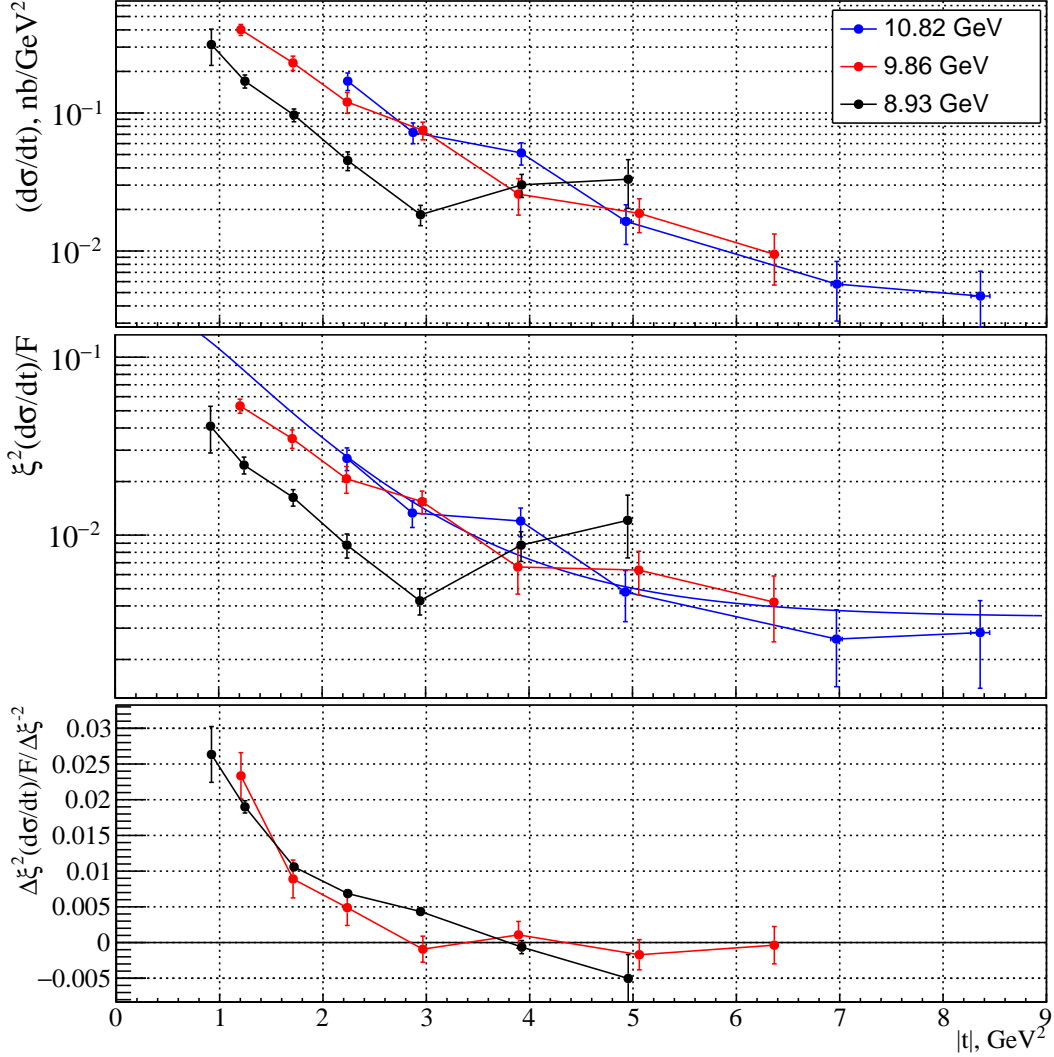
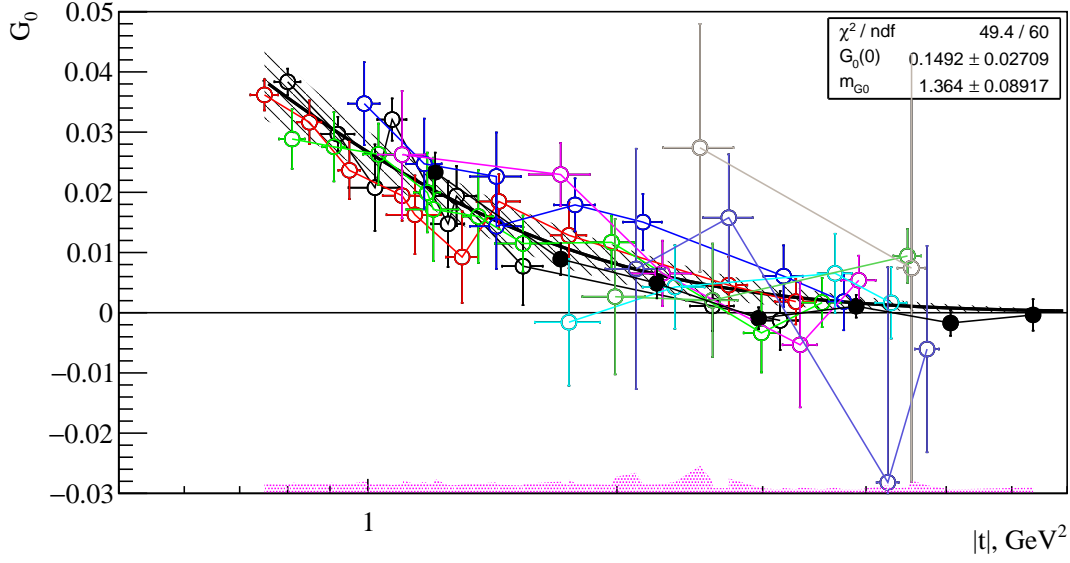


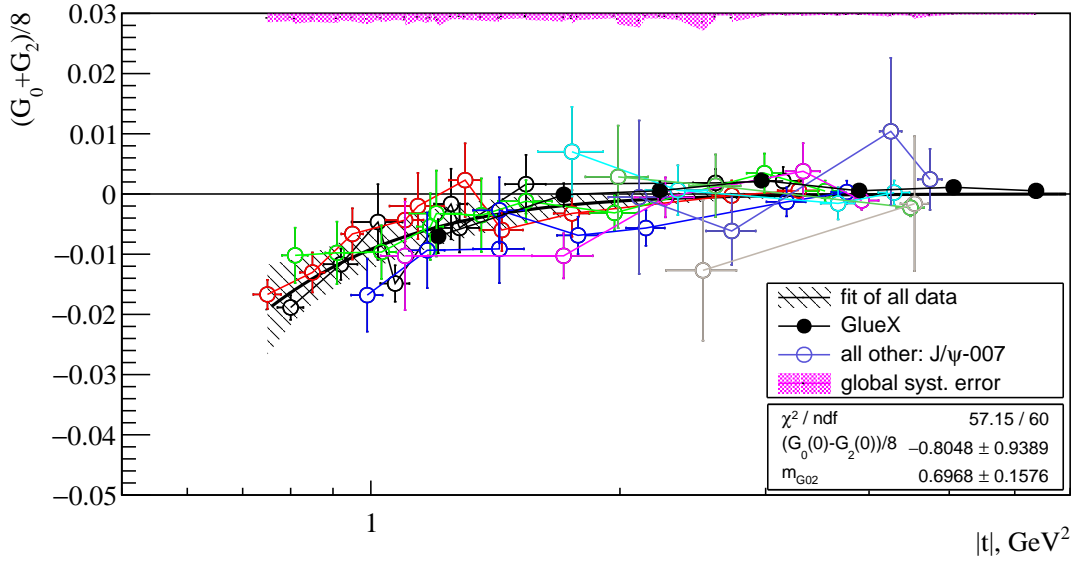
FIG. 3: Different stages of applying the “Rosenbluth” extraction of the  $G_0(t)$  function using the GlueX data: the differential cross sections at three energy slices (top), the reduced cross sections - Eq.(22) (middle), and the extracted  $G_0(t)$  function with Eq.(24) using the highest energy as a reference (bottom). The fitted function of the reduced cross section at the highest energy from the global fit (Fig.2 bottom right), is shown in the middle panel (blue curve), as well. The points are connected with lines to guide the eye only.

function is extracted as:

$$H_0^{exp.}(t) = [\sigma_{H0}(E_i, t) - \sigma_{H0}(E_j, t)] / [\eta^{-2}(E_i, t) - \eta^{-2}(E_j, t)], \quad (29)$$



(a)



(b)

FIG. 4:  $G_0(t)$  (top) and  $(G_0(t) + G_2(t))/8$  (bottom) functions as extracted from the GlueX (solid) and  $J/\psi$ -007 (open symbols) data for  $\xi > 0.4$  using Eqs.(24,25) for different photon beam energies (different colors connected with lines). The data points are fitted with squared dipole functions,  $G(0)/(1 - t/m_G^2)^4$ , shown with confidence range at 95% confidence level.

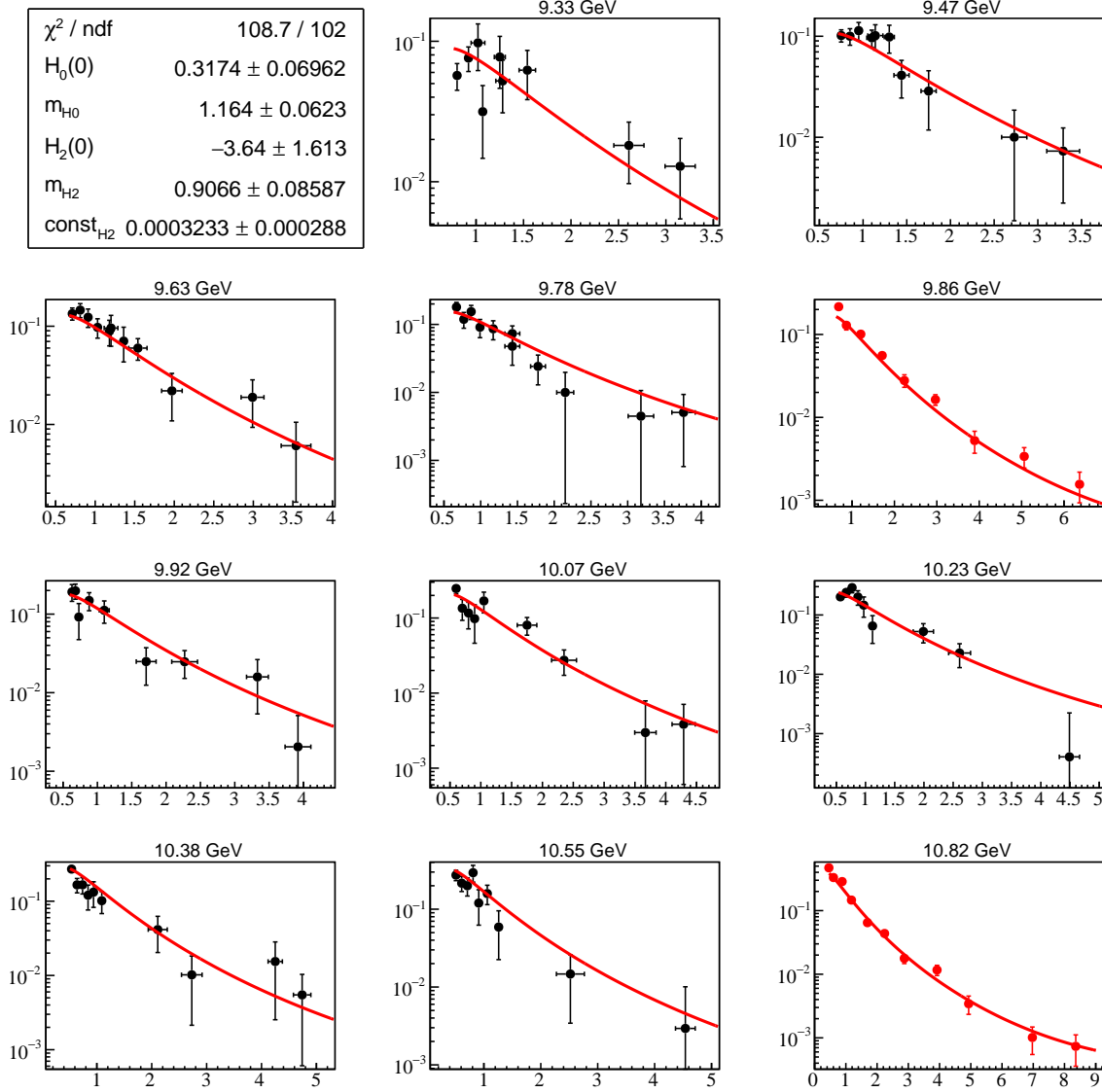


FIG. 5: Global five-parameter fit of the reduced cross sections,  $\eta^{-2}/N \cdot d\sigma/dt$ , as function of  $|t|$  (in  $\text{GeV}^2$ ), using the holographic Eq.(14), from GlueX (red) and  $J/\psi$ -007 (black) experiments for different photon energies as indicated. For the further analysis only the fitted function at 10.82 GeV is used.

where the corresponding reduced cross section is defined as:

$$\sigma_{H0}(E, t) = \frac{d\sigma}{dt}(E, t) \frac{\eta^{-2}(E, t)}{N(E)}. \quad (30)$$

When compared to the GPD calculations, the difference comes from the extra  $\xi^{-4}$  prefactor in Eq. (1).

Following the same procedure as in the case of the GPD analysis, we perform global fit of the reduced cross sections using Eq. (14), where  $H_0$  and  $H_2$  functions are parametrized in the same way as  $G_0$  and  $G_2$  in Eqs. (27,28) and  $H_4$  is neglected. The most important difference is that in the holographic case all the data points with  $E > 9.3$  GeV are included in the fit and there is no need to extrapolate the reference cross section at  $E_i = 10.82$  GeV as its  $t$ -range covers the range of all the other measurements, see Fig. 1. The fit results shown in Fig. 5 demonstrate good fit quality.

We extract the  $H_2$  function in a very similar way:

$$H_2^{exp.}(t) = [\sigma_{H_2}(E_i, t) - \sigma_{H_2}(E_j, t)] / [\eta^2(E_i, t) - \eta^2(E_j, t)], \quad (31)$$

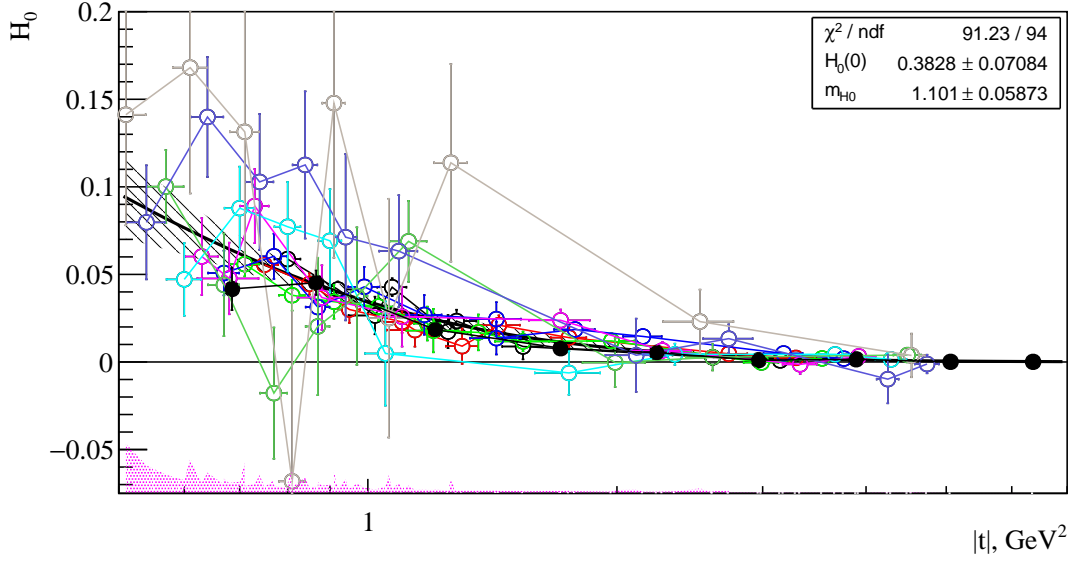
where the corresponding reduced cross section is just the normalized differential cross section:

$$\sigma_{H_2}(E, t) = \frac{d\sigma}{dt}(E, t) \frac{1}{N(E)}. \quad (32)$$

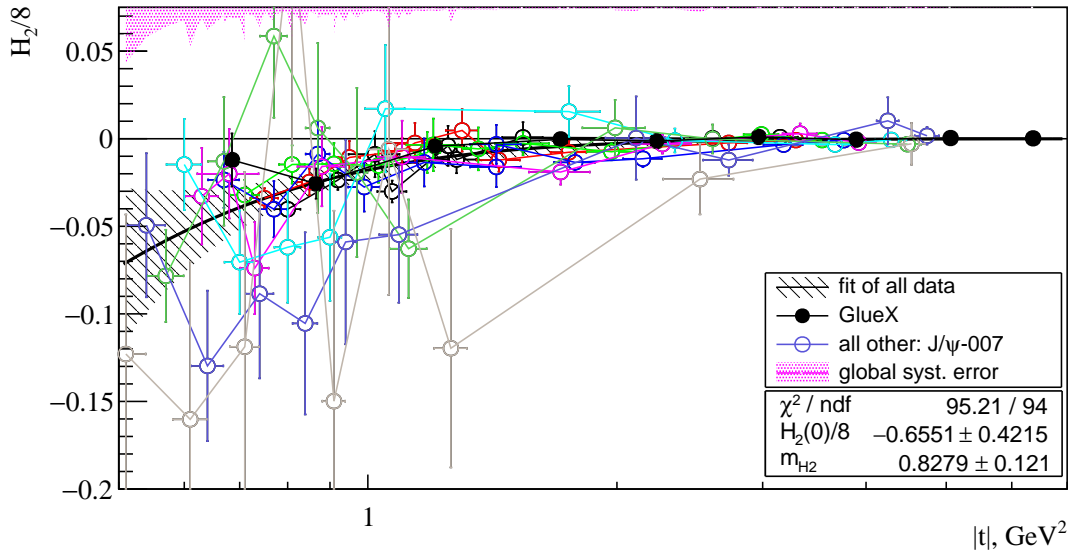
The results for the extracted  $H_0$  and  $H_2$  form factor functions are shown in Fig. 6. They are fitted with squared dipole functions, demonstrating that in the case of the holographic calculations, the extracted data points are also energy independent. As there is no constraint on the skewness parameter, the extracted form factor functions extend down to lower  $|t|$  values, as compared to the GPD case. Note, however, that in the low  $|t|$  region the errors are much bigger than in the GPD analysis, as the errors of the measurements are scaled by bigger factors in Eqs.(30,32), compared to Eqs.(22,26), in the corresponding reduced cross sections.

#### IV. RELATION TO THE GLUON GRAVITATIONAL FORM FACTORS

In the leading-moment approximation the  $G$  functions are related to the gGFFs according to Eqs.(19-21), where we have neglected the  $B_g$  form factor. In case of the holographic theory, if the required conditions for the theory to be valid are met, the  $H$  functions are related to the gGFFs as given by Eqs.(15-17).



(a)



(b)

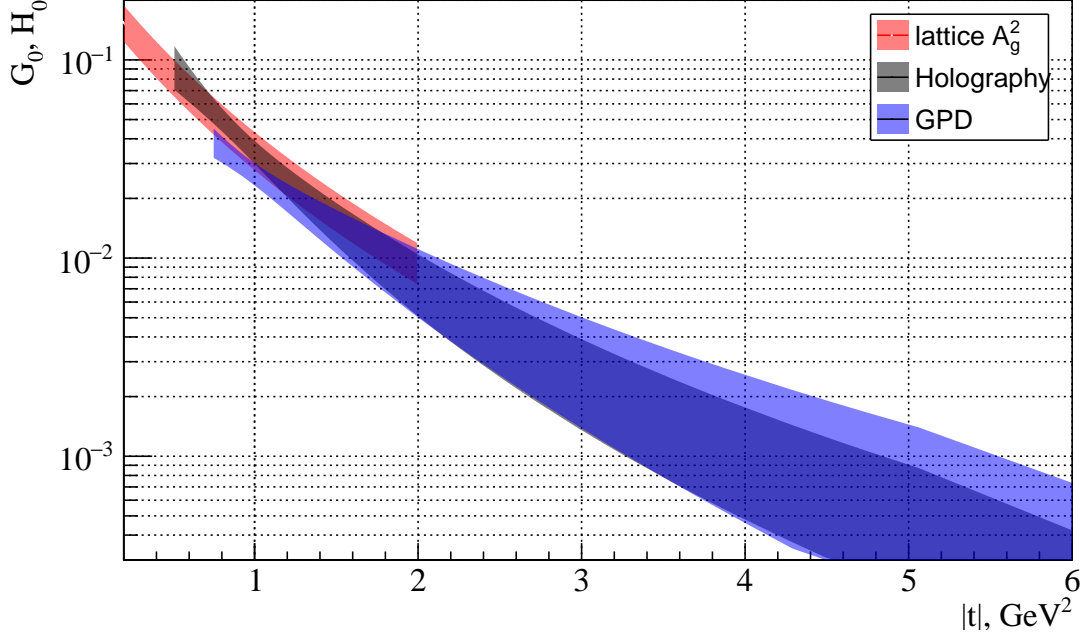
FIG. 6:  $H_0(t)$  (top) and  $H_2(t)/8$  (bottom) functions as extracted from the GlueX (solid) and  $J/\psi$ -007 (open symbols) data using Eqs.(29,31) for different photon beam energies (different colors connected with lines). The data points are fitted with squared dipole functions,  $H(0)/(1 - t/m_H^2)^4$ , shown with confidence range at 95% confidence level.



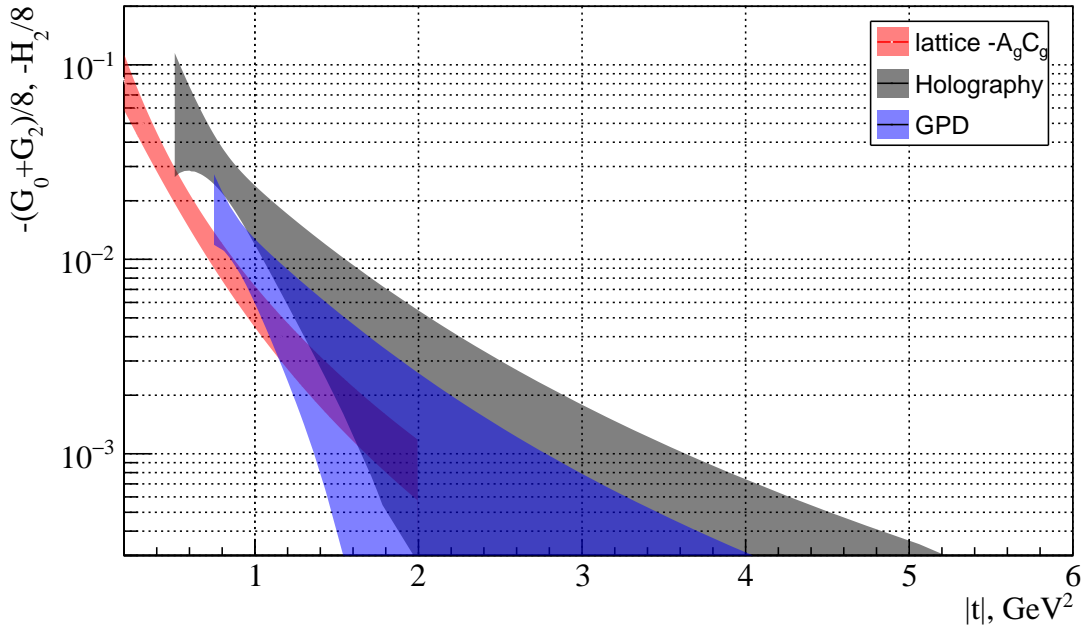
In Fig. 7a we compare the functions fitted to the data points (as extracted in the previous section) for  $G_0$  and  $H_0$ . We see a general agreement between the GPD and holographic results, which is remarkable as these two theories are diametrically different. A possible way to interpret their agreement is that the corrections to both theories, which have very different nature, are not dominant. Indeed, according to Eqs.(19,15), the leading terms of both,  $G_0$  and  $H_0$ , are the same and equal to the  $A_g$  form factor squared. This assumption is supported by comparing the experimental results to the lattice calculations of  $A_g^2$  from Ref. [13] (shown in the same figure), where we see an agreement at least within  $2\sigma$  in the common  $0.5 - 2 \text{ GeV}^2$  region.

In case of the  $G_0 + G_2$  and  $H_0$  their leading terms should be proportional to the product of the gGFFs  $A_g C_g$  (Eqs.(20,16)). The functions fitted to data points for  $(G_0 + G_2)/8$  and  $H_0/8$  from the previous section are shown in Fig. 7b and compared to the lattice calculation of  $A_g C_g$ . The agreement is not as good as in the  $A_g^2$  case, at the same time the uncertainties of the data are much bigger so that we cannot make a definitive conclusion.

We will discuss the vanishing of the terms containing  $G_4$  and  $H_4$  in Eqs.(18,14) within the leading-term approximation used in this section. Note that the mass scale parameter for  $G_0$  is bigger than the one for  $G_0 + G_2$ ,  $m_{G_0} > m_{G_0+G_2}$  (Fig. 4). The same is true when comparing the results for  $H_0$  and  $H_2$ :  $m_{H_0} > m_{H_2}$  (Fig. 6). According to Eqs.(19,20) and Eqs.(15,16), this means that  $C_g$  vanishes faster with  $|t|$  than  $A_g$ . As  $G_4$  and  $H_4$  are proportional to  $C_g^2$  (Eqs.(21,17)), this explains qualitatively their vanishing contribution in Eqs.(18,14) at high  $|t|$  values. At low  $|t|$  where  $\xi$  and  $\eta$  are much smaller than unity, these terms are suppressed by the  $\xi^4/\xi^2$ , or  $\eta^4/\eta^2$  factors when compared to the first/second term in Eqs.(18,14). From the extracted  $A_g^2$  and  $A_g C_g$  combinations we can evaluate separately the  $C_g$  form factor and then calculate the  $G_4$  and  $H_4$  functions using Eqs.(21,17). In this way we have verified quantitatively, based on the results in this paper, that for  $|t| > 0.7 \text{ GeV}^2$ ,  $\xi^4 G_4$  is much smaller in absolute value than  $G_0$  and  $\xi^2 G_2$ . The same is true in the holographic case:  $\eta^4 H_4$  is much smaller in absolute value than  $H_0$  and  $\eta^2 H_2$  for  $|t| > 0.5 \text{ GeV}^2$ . Thus, in the leading-term approximation, this justifies neglecting the  $G_4/H_4$  terms when extracting the form factors.



(a)



(b)

FIG. 7: Comparison of the functions fitted to the extracted data points from Figs. 4,6 with the corresponding lattice calculations of Ref. [13]: (top)  $G_0$ ,  $H_0$ , compared to  $A_g^2$  from lattice, (bottom)  $-(G_0 + G_2)/8$ ,  $-H_2/8$ , compared to  $-A_g C_g$  from lattice. All the uncertainty bands correspond to 95% confidence level.

## V. ADDITIONAL REMARKS AND SUMMARY

An interesting result can be deduced from the general  $\xi$ -scaling expression, Eq.(1), though not directly related to the extraction of the form factors. First, we note that  $G_0$  must be positive as a sum of squares of  $\mathcal{A}_g$  and  $\mathcal{B}_g$  functions, according to Eq.(6) with  $t$  being negative. Therefore, from Eq.(24), for  $E_i > E_j$  at a fixed  $t$ , as  $\xi(E_i, t) < \xi(E_j, t)$  and therefore  $\xi^{-2}(E_i, t) - \xi^{-2}(E_j, t) > 0$ , it follows that:

$$d\sigma/dt(E_i, t) \frac{\xi^2(E_i, t)}{F(E_i)} > d\sigma/dt(E_j, t) \frac{\xi^2(E_j, t)}{F(E_j)}, \quad E_i > E_j. \quad (33)$$

In particular, as  $\xi^2(E_i, t)/F(E_i) < \xi^2(E_j, t)/F(E_j)$ ,<sup>2</sup> it means that:

$$d\sigma/dt(E_i, t) > d\sigma/dt(E_j, t), \quad E_i > E_j. \quad (34)$$

In other words, the differential cross section at a fixed  $t$  must increase with the energy, something that is not trivial.

In the GPD approach our ‘‘Rosenbluth’’ procedure relies on Eq.(1) that comes in Ref. [1] from some general theoretical assumptions about the  $J/\psi$  photoproduction mechanisms, such as gluon exchange and factorization. The observation of the energy independence of the extracted  $G$  form factor functions means that the experimental data, within their uncertainties, are consistent with the assumptions in Ref. [1]. In the holographic case, Eq.(2), which relates directly  $d\sigma/dt$  to the gGFFs can be interpreted as a more general expression in powers of  $\eta$  as in Eq.(14). The energy independence of the extracted  $H$  functions supports such an interpretation within the errors of the present data set. We stress that these results are based only on Eqs.(1,14) and no additional information is used. Note that any constraints on the gGFF like fixing parameters on their parametrizations depend on the assumption of a leading-term approximation.

The results from the ‘‘Rosenbluth’’ separation for the parameters of the functions fitted to  $G_0$ ,  $H_0$ , and  $H_2$  (Figs. 4,6) and the results of the global fits in Figs. 2,5 are consistent with

---

<sup>2</sup> This inequality follows from Eq.(5) and the kinematical factor  $F(E)$  being proportional to  $1/(s - m^2)^2$  [1].

each other<sup>3</sup>. This is a result of using the same data set and the same parametrization for the  $G$  and  $H$  functions. However, these two methods of extracting the  $G$  and  $H$  functions are not equivalent. The global fits assume a priori the functional forms used to parametrize the  $G$  and  $H$  functions. The “Rosenbluth” separation uses only the function fitted to the reference data set. The global fits to all the data used in this case are needed to reduce the systematic errors and, in the GPD case, to extrapolate the reference data to lower  $|t|$  values. In the holographic case we can extract the  $H$  functions by interpolating the reference cross section without performing a global fit of all the data. The fit of the data points extracted in this way is used to infer (rather than assume) the proper functional form, a squared dipole function, used in the global fits of the reduced cross sections.

We conclude, based on the analysis of the current experimental data (Fig.4), that the  $\xi$ -scaling behavior is valid for  $\xi > 0.4$ . As discussed in Ref. [1], such a low limit is not justified theoretically and may result in a significant bias. However, this value should be considered as a lower limit of the validity of the  $\xi$ -scaling, as more precise data could move this value up.

In Fig. 7 we have compared the extracted  $G$  and  $H$  functions with the calculations in the leading-term approximation when using lattice gGFFs. The procedure described in this paper does not use any external constraints and does not depend on the absolute normalization of the corresponding theoretical calculations. The absolute value of the extracted form factor functions comes from the data - more precisely from the slope of the differential cross section as a function of the energy. Therefore we find it remarkable that the data points obtained with two diametric theories are on the same scale as the lattice results. If with higher statistics the agreement between the data and lattice calculations in the overlapping  $t$ -region is confirmed, this could justify the extraction of the gGFFs at high  $t$  directly from the data, complementary to the lattice results available at low  $t$ .

It is critical to further investigate the near-threshold region of  $E < 9.3$  GeV. For that we would need more statistics and further theoretical and phenomenological studies to understand the possible contribution of open charm channels. If gluon exchange still dominates

---

<sup>3</sup> The “Rosenbluth” results for  $G_2$  are also consistent with the fit parameters in Fig. 2. For the sake of focusing on the analogy between the GPD and holographic approaches, these results are not shown in the paper, as it is the sum  $G_0 + G_2$  that has the same relation to the gGFFs as the  $H_2$  function.

at least in some kinematic region, it will be very important to have this region included in the presented analysis. It is believed that close to threshold, being close to both  $|t|_{min}$  and  $|t|_{max}$  kinematic limits, the factorization would be better justified, at the same time the higher  $\xi$  values in this region would better satisfy the requirements for the high- $\xi$  expansion in Ref.[1].

The results in this paper should not be understood as a proof of the validity of the assumptions in Ref. [1] and Ref. [2], rather just as an indication, within the present data uncertainties, of the validity of the scaling as defined by Eqs.(1,14). Such scaling behavior as demonstrated experimentally in this work can be considered as an independent phenomenological observation possibly coming from some more general theoretical assumptions. In any case, the presented results are encouraging and should stimulate the continuation of the experimental studies and further theoretical analysis.

## VI. ACKNOWLEDGMENTS

We would like to thank Yuxun Guo and Ismail Zahed for the fruitful discussions and explanations of the theories on which the results of this work are based and Simon Taylor for valuable comments.

Notice: Authored by Jefferson Science Associates, LL under U.S. DOE Contract No. DE-AC05-06OR23177. The U.S. Government retains a non-exclusive, paid-up, Eire- vocable, world-wide license to publish or reproduce this manuscript for U.S. Government purposes.

- 
- [1] Y. Guo, X. Ji, and F. Yuan, Phys. Rev. D **109**, 014014 (2024).
  - [2] K. A. Mamo and I. Zahed, Phys. Rev. D **106**, 086004 (2022).
  - [3] S. J. Brodsky and G. A. Miller, Physics Letters B **412**, 125 (1997).
  - [4] P. Sun, X.-B. Tong, and F. Yuan, Physics Letters B **822**, 136655 (2021).
  - [5] Y. Guo, X. Ji, and Y. Liu, Physical Review D **103** (2021), 10.1103/physrevd.103.096010.
  - [6] Y. Guo, X. Ji, Y. Liu, and J. Yang, Physical Review D **108** (2023), 10.1103/phys-

revd.108.034003.

- [7] Y. Hatta and M. Strikman, Phys. Lett. B **817**, 136295 (2021).
- [8] A. Ali et al. (GlueX collaboration), Phys. Rev. Lett. **123**, 072001 (2019).
- [9] S. Adhikari et al. (GlueX collaboration), Physical Review C **108** (2023), 10.1103/physrevc.108.025201.
- [10] B. Duran et al. ( $J/\psi$ -007 collaboration), Nature **615**, 813 (2023).
- [11] L. Frankfurt and M. Strikman, Phys. Rev. D **66**, 031502 (2002).
- [12] D. A. Pefkou, D. C. Hackett, and P. E. Shanahan, Physical Review D **105** (2022), 10.1103/physrevd.105.054509.
- [13] D. C. Hackett, D. A. Pefkou, and P. E. Shanahan, “Gravitational form factors of the proton from lattice qcd,” (2023), arXiv:2310.08484 [hep-lat].
- [14] M. N. Rosenbluth, Phys. Rev. **79**, 615 (1950).
- [15] M.-L. Du, V. Baru, F.-K. Guo, C. Hanhart, U.-G. Meißner, A. Nefediev, and I. Strakovsky, Eur.Phys.J.C **80** (2020), 10.1140/epjc/s10052-020-08620-5.
- [16] D. Winney, C. Fernández-Ramírez, A. Pilloni, A. N. Hiller Blin, M. Albaladejo, L. Bibrzycki, N. Hammoud, J. Liao, V. Mathieu, G. Montaña, R. J. Perry, V. Shastry, W. A. Smith, and A. P. Szczepaniak (Joint Physics Analysis Center), Phys. Rev. D **108**, 054018 (2023).